



HAL
open science

In Silico Exploration of Bisphosphonate Scaffolds as Potential Inhibitors of SARS-CoV-2 RdRp for COVID-19 and PASC

Muzaffar-Ur-Rehman Mohammed, Suryakant Chougule, Chandu Ala, Pranali Vijaykumar Kuthe, Mohit Garg, Murugesan Sankaranarayanan, Seshadri S Vasana

► **To cite this version:**

Muzaffar-Ur-Rehman Mohammed, Suryakant Chougule, Chandu Ala, Pranali Vijaykumar Kuthe, Mohit Garg, et al.. In Silico Exploration of Bisphosphonate Scaffolds as Potential Inhibitors of SARS-CoV-2 RdRp for COVID-19 and PASC. Pathogens, In press. hal-04365275

HAL Id: hal-04365275

<https://hal.science/hal-04365275>

Submitted on 27 Dec 2023



HAL is a multi-disciplinary open access archive for the deposit and dissemination of scientific research documents, whether they are published or not. The documents may come from teaching and research institutions in France or abroad, or from public or private research centers.

L'archive ouverte pluridisciplinaire **HAL**, est destinée au dépôt et à la diffusion de documents scientifiques de niveau recherche, publiés ou non, émanant des établissements d'enseignement et de recherche français ou étrangers, des laboratoires publics ou privés.



Distributed under a Creative Commons Attribution - NonCommercial 4.0 International License

1 Article

2 **In Silico Exploration of Bisphosphonate Scaffolds as Potential**
3 **Inhibitors of SARS-CoV-2 RdRp for COVID-19 and PASC**4 Muzaffar-Ur-Rehman Mohammed ¹ ‡, Kishor Suryakant Chougule ¹ ‡, Chandu Ala ¹, Pranali Vijaykumar Kuthe ¹,
5 Mohit Garg ², Murugesan Sankaranarayanan ^{1*} , and Seshadri S. Vasani ^{3,4*} 6 ¹ Department of Pharmacy, Birla Institute of Technology and Science, Pilani 333031, India7 ² Department of Chemical Engineering, Birla Institute of Technology and Science, Pilani 333031, India8 ³ School of Medical and Health Sciences, Edith Cowan University, Joondalup, WA 6027, Australia9 ⁴ Department of Health Sciences, University of York, York YO10 5DD, U.K.10
11 * Correspondence: murugesan@pilani.bits-pilani.ac.in or prof.vasani@york.ac.uk

12 ‡ These authors contributed equally to this work.

13 **Abstract:** The novel coronavirus disease (COVID-19) pandemic has resulted in over 720 million
14 confirmed cases and 7 million deaths worldwide, with insufficient treatment options. Innumerable
15 efforts are being made around the world for faster identification of therapeutic agents to treat the
16 deadly disease. Postacute sequelae of SARS-CoV-2 infection or COVID-19 (PASC), also called Long
17 COVID, is still being understood and lacks treatment options as well. A growing list of drugs are
18 being suggested by various *in silico*, *in vitro* and *ex vivo* models, however currently only two treat-
19 ment options are widely used: the RNA-dependent RNA polymerase (RdRp) inhibitor remdesivir,
20 and the main protease inhibitor nirmatrelvir in combination with ritonavir. Computational drug
21 development tools and *in silico* studies involving molecular docking, molecular dynamics, entropy
22 calculations and pharmacokinetics can be useful to identify new targets to treat COVID-19 and
23 PASC, as shown in this paper. We have investigated bisphosphonates which can bind competi-
24 tively to nidovirus RdRp-associated nucleotidyl (NiRAN) transferase domain, and systematically
25 down selected seven candidates for further evaluation (ChEMBL608526, ChEMBL196676,
26 ChEMBL164344, ChEMBL4291724, ChEMBL4569308, ChEMBL387132, ChEMBL98211). Inter-
27 estingly, one of these (ChEMBL608526) very closely resembles the approved drug minodronate,
28 and another (ChEMBL98211) resembles the approved drug zoledronate.29 **Keywords:** Bisphosphonates; Long COVID; Minodronate; MM-GBSA; Molecular docking; Molec-
30 ular dynamics; RdRp; SARS-CoV-2; Virtual screening; Zoledronate.

31

Citation: To be added by editorial
staff during production.Academic Editor: Firstname
Lastname

Received: date

Revised: date

Accepted: date

Published: date

32
33
34
35
36
37
38
39
40
41
42
43
44
45
Copyright: © 2023 by the authors.
Submitted for possible open access
publication under the terms and
conditions of the Creative Commons
Attribution (CC BY) license
(<https://creativecommons.org/licenses/by/4.0/>).32 **1. Introduction**33 Coronaviruses are responsible for causing seasonal respiratory tract infections in
34 people and are associated with common cold symptoms [1]. The highly pathogenic hu-
35 man coronaviruses (HCoVs) such as severe acute respiratory syndrome (SARS) associ-
36 ated coronavirus (SARS-CoV), Middle East respiratory syndrome-related coronavirus
37 (MERS-CoV) and the novel SARS-CoV-2 cause infection to epithelial cells of the bronchi
38 and pneumocytes, which could lead to life-threatening lung injuries [2]. Among these
39 three, the SARS-CoV-2 virus which emerged in December 2019 exhibits faster hu-
40 man-to-human transmission, and resulted in over 780 million confirmed cases and 7
41 million reported deaths due to the novel coronavirus disease (COVID-19) [3]. Long
42 COVID, also known as postacute sequelae of SARS-CoV-2 infection or COVID-19 (PASC)
43 [4,5], may affect typically 3.1% of the population, especially those aged 35 to 69 years,
44 females, people living in more deprived areas, those working in social care, those aged 16
45 years or over who were not working and not looking for work, and those with another

46 activity-limiting health condition or disability [6].

47 SARS-CoV-2 employs a multi-subunit machinery for replication and transcription.
48 Non-structural proteins (Nsp's) produced as cleavage products due to the open reading
49 frame 1a and 1b (ORF1a and ORF1b) facilitate viral replication and transcription [7]. One
50 of these, known as Nsp12 or RNA-dependent RNA polymerase (RdRp), catalyzes the
51 synthesis of viral RNA and plays a central role in the replication and transcription cycle
52 of SARS-CoV-2 with Nsp7 and Nsp8 as co-factors [8,9]. Therefore, Nsp12 is considered a
53 primary target for antiviral agents, with the potential for treating COVID-19 [10], and
54 possibly other coronaviral diseases because it is a highly conserved motif. For example,
55 sequence alignment results from the literature shows 96% common identity between
56 SARS-CoV and SARS-CoV-2 [11].

57 In this work, as we shall be using RdRp as a key target let us first describe its com-
58 ponents: it has the Nsp12 catalytic subunit, two accessory subunits (Nsp8 and Nsp7), and
59 more than two turns of RNA template-product duplex [12]. The RdRp domain is analo-
60 gous to a cupped right hand, consisting of the finger 'F' (amino acid residues 398–581,
61 628–687), palm (amino acid residues 582–627, 688–815) and thumb (amino acid residues
62 816–919) subdomains found in all single-subunit polymerases [13]. An in-depth struc-
63 tural analysis depicts the Nsp12 subunit binding to the first turn of RNA between its F
64 and thumb sub-domains. The core protein consists of a single chain of 942 amino acids.
65 The active site comprises of five conserved Nsp12 elements that are found in the palm
66 motif. The amino acids Asp760 and Asp761 (Figure 1) are necessary for synthesis, which
67 binds to the 3' end of the RNA. The RNA template is positioned by the supplementary
68 Nsp12 finger motif. The second turn is positioned by two copies of Nsp8 that bind to the
69 cleft on the opposite sides. As RNA exits, large helical extensions of Nsp8 protrude and
70 create positively charged sliding poles that are necessary for coronaviruses to replicate
71 their lengthy genomes [14]. Structural stability requires two Zinc (Zn) ions interacting
72 with the residues present in the N-terminal domain (His295, Cys301, Cys306, Cys310)
73 and finger domain (Cys487, His642, Cys645, Cys646). The presence of Zn in this site in-
74 dicates its crucial role in stabilizing the overall 3D structure of the protein [15]. The
75 binding of drugs to the amino acid residues in motif F of RdRp averts the entry of the
76 substrate and divalent cations into the central active site cavity, thereby inhibiting the
77 catalytic activity of the enzyme and preventing the RNA replication [16].

78 So far, the standard drugs of choice for treatment have been the emergency use au-
79 thorized (EUA) drugs, nirmatrelvir and remdesivir. Nirmatrelvir is an orally available
80 main protease (M^{pro}) inhibitor [17], while remdesivir is an RdRp inhibitor that is admin-
81 istered parenterally. The EUA status of remdesivir was revoked on April 2022, and ap-
82 proval as a supplemental new drug application has been given in December 2022 [16].
83 However, a recent study published in *The Lancet* shows that while remdesivir could re-
84 duce the risk it had an insignificant effect in ventilated COVID-19 patients [17].
85 Nirmatrelvir, a main protease inhibitor, exhibited promising antiviral effects but was
86 susceptible to rapid degradation. To mitigate this issue, ritonavir, a protease inhibitor,
87 was incorporated in a combined formulation which received FDA approval as the first
88 oral antiviral pill PAXLOVID [18]. Other drugs that have shown promise include
89 molnupiravir [19], favipiravir [20] and fluvoxamine [21,22]. However, molnupiravir and
90 favipiravir are no longer recommended as the former drug has poor clinical outcomes
91 [23–25] and the latter showed ineffective in viral clearance [26–28]. Although fluvoxam-
92 ine has been shown to have both immunomodulatory effects [29] as well as antiviral ef-
93 fects [21,30,31], it is clear that this drug can only be used in combination and not in its
94 own [21,29].

Therefore, the quest to identify potential molecules to treat COVID-19 and PASC is still ongoing [32]. In the literature, when databases of molecules including synthetic and natural origin were screened against RdRp [33–40] together with other non-structural proteins (Nsp's) inhibitors [41–44], these studies were looking for better alternatives to remdesivir. Few studies also reported the screening of analogues of different scaffolds such as quinolines [40], cytidines [45] and andrographolides [46]. It's also common for repurposing efforts to propose drugs that are yet to be tested *in vitro* [13,32,38–40,47–53]. As RdRp is a key target, this paper looks at a class of small molecules called bisphosphonates (BPs) for five reasons: 1. The use of selected BPs is associated with a 3-5 fold reduction in the incidence of SARS-CoV-2 testing, COVID-19 diagnosis, and related hospitalization during the pandemic [54,55]; 2. BP scaffolds exhibit competitive binding to the nidovirus RdRp-associated nucleotidyl (NiRAN) transferase domain [56]; 3. Our prior experience with an immunomodulatory drug, fluvoxamine, in different (*in silico*, *in vitro* and *ex vivo*) studies [21]; 4. Our recent study which has shown that alendronate, a BP drug, has promising *in silico* results compared to remdesivir [32]; and 5. BPs benefit the age groups that also experience severe forms of COVID-19. Therefore, we shall further explore BPs in detail as it is the focus of this follow-up study.

BPs are a class of small-molecule drugs that have two phosphonate groups. They are categorized into nitrogen-containing (amino-BPs) and nitrogen-free BPs (non-amino-BPs). They are mainly used to treat osteoporosis, Paget's disease of the bone, and to lower high calcium levels in people with cancer [57]. In addition, amino-BPs control the activation, expansion, and function of a significant portion of human $\gamma\delta$ T cells (i.e., it reduces the amount of circulation $\gamma\delta$ T cells), as well as neutrophils, monocytes and macrophages. They can also modify the dendritic cell's ability to present antigens to the immune system. Results from animal experiments indicate that both amino-BPs and non-amino-BPs have strong adjuvant-like effects of increasing antibody and T-cell responses to viral antigens. [58]. Such a range of immunomodulatory effects and the drug's binding with RdRp inspired us to investigate BPs as prospective COVID-19 and/or PASC drug candidates [54,56,58].

2. Materials and Methods

In this study, a series of compounds having BPs were downloaded from the ChEMBL database [59] and molecular docking study was carried out to get all the “hit” molecules. These hits were further down-selected using molecular mechanics with generalized Born and surface area (MM-GBSA) studies and the top seven ligands were analyzed for their dynamic behavior via molecular dynamics studies followed by the entropic calculations using the software “gromacs” (v2022.4).

2.1. Protein Preparation

While the literature shows a high sequence identity (96%) between the RdRp proteins of SARS-CoV and SARS-CoV-2, we couldn't find any report with MERS-CoV, so the latter's RdRp domain (residues 4845–5412 from accession code A0A023YA54) was taken and multiple sequence alignment was carried out to reveal the conserved motifs (75%) for these three coronaviruses (Figure 1). To start screening BPs against SARS-CoV-2, RdRp protein (PDB: 6M71) [8] was selected and downloaded from the protein data bank (<https://www.rcsb.org/>). The protein was prepared using the protein preparation wizard of the glide module of the Schrödinger software (Schrödinger LLC., NY, v2022) [60]. Missing hydrogens and residues were added using the software's prime module and pre-processed using the Epik module at pH 7.0±2.0 [61]. The protein was optimized by removing water molecules beyond 3 Å and subjected to minimization using the optimized potentials for liquid simulations 4 (OPLS4) force field [61].

2.2. Ligand preparation

ChEMBL database has been used to download molecules containing BPs based on the Tanimoto similarity check (95%) [44]. These molecules were imported and prepared using Ligprep module of maestro (Schrödinger LLC., NY, v2022). The ionization state was set to neutral and chirality was determined from the 3D structure. The force field OPLS4 was employed to prepare the ligands.

2.3. Molecular docking

For carrying out molecular docking studies, a grid box of 10 Å³ was generated using the maestro receptor grid generation wizard (Schrödinger) by specifying the binding (active) site residue Arg555, as no co-crystal ligand was available [49]. The ligands were docked using the ligand docking wizard of the glide module of Schrödinger with standard-precision (SP) mode initially. The molecules that were able to bind were subjected to filtration by applying the criterion of molecular weight (<500 Da) and number of rotatable bonds (<10) [63]. Molecules obtained from this filtration process were then subjected to docking with extra-precision (XP) mode [64].

2.4. MM-GBSA calculations

Molecular mechanics with generalised Born and surface area solvation (MM-GBSA) studies help to calculate the ligand's binding-free energy (ΔG_{bind}) value. The calculations were mainly based on the summation of differences in the minimization (ΔE_{MM}), solvation (ΔG_{Solv}), and surface area (ΔG_{SA}) energies of RdRp-ligand complex structure and free RdRp and ligand molecules [65]. The protein-ligand complex from the docking studies was used to calculate the binding free energy. The analysis was carried out in the prime module of Schrödinger software. OPLS4 force field with dielectric surface generalized Born (VSGB) continuum solvation model was used. Based on the following formula, the binding free energy of the ligand was calculated:

$$\Delta G_{\text{bind}} = \Delta E_{\text{MM}} + \Delta G_{\text{Solv}} + \Delta G_{\text{SA}} \dots \dots \dots (1)$$

2.5. Molecular dynamics studies

The molecular dynamics (MD) simulation was accomplished to determine the ligand and molecules' stability, confirmation and intermolecular interaction with the target RdRp protein (PDB ID: 6M71) [66]. The time-dependent modification of the complexes was estimated over 100 ns using the Desmond module. The MD simulation was executed at a constant temperature of 310 K using Nosé-Hoover chain thermostat, and constant pressure of 1.013 bar using Martyna-Tobias-Klein barostat [67,68]. The complete system was annealed and equilibrated using ensembles.

The down-selected ligand complexes were imported and prepared using the protein preparation wizard of the Desmond module (Schrödinger LLC., NY, v2020). The complex was solvated using the transferable intermolecular potential with 3 points (TIP3P) model and the grid boundary dimensions was set to 10 Å³ [69]. The complex model was electrically neutralized with Na⁺/Cl⁻ ions, and built using a system builder wizard. The complete solvated model was minimized and molecular dynamics was carried out for 100 ns on all eight selected complexes (including the reference drug remdesivir, and the negative control cinnamaldehyde). The root mean square deviation (RMSD), root mean square fluctuation (RMSF) and interaction plots were used to interpret the stability of appropriate complexes.

2.6. Entropy calculation for molecular dynamics trajectories

The binding free energy of the protein-ligand complex was determined using the gmx_mmPBSA tool [70,71]. In this calculation, the molecular mechanism Pois-

son-Boltzmann surface area (MMPBSA) method with a dielectric model (“ipb” = 2) and a non-polar solvation model (“inp” = 1) were employed. The ionic strength of the surrounding medium was maintained at 0.15 M, and the temperature was set at 310 K. To calculate the entropy (-TΔS), the interaction entropy (I.E.) method was used [72]. This allowed us to evaluate the change in binding free energies with entropy contributions for the protein, ligand, and their complexes. The trajectories from the protein-ligand MD simulation in explicit water from the Desmond module were used to generate the gromacs trajectory file required for calculations using visual molecular dynamics (VMD) software. Additionally, topology files for protein and ligand were obtained separately by converting the *.cms files to *.gro and *.top files using the intermol software [73]. Since the initial frames during the dynamic simulation are involved in the equilibrium, the frames after 50 ns were considered for data analysis. To speed up the procedure and to get better averaging, we ran five independent MMPBSA calculations (10 ns each) for every complex from 50-100 ns and reported the average and standard deviation of these calculations [74].

2.7. ADMET (absorption, distribution, metabolism, excretion, toxicity) studies

To determine the pharmacokinetic and pharmacodynamic profiles, the smiles format of the hit compounds was used and their parameters were predicted using the pkCSM web-tool [75]. All the absorption, distribution, metabolism, excretion and toxicity parameters obtained were compared with the standard reference drug remdesivir.

3. Results and Discussion

All the drug molecules (synthetic and approved) obtained from the ChEMBL database were docked into the binding site of the RdRP protein (PDB ID: 6M71) using the ligand docking wizard of the glide module of Schrödinger software. The test molecules were docked using the SP mode and we obtained 1,992 molecules, signifying that all test molecules have occupied the active site pocket. Larger molecules >500 Daltons find it harder to absorb as smaller molecules are more absorbable. Hence, we used molecular weight (<500 Daltons) to filter out large molecules. The number of drugs that passed the filter was 1,398. To further reduce this number, a filter corresponding to the number of rotatable bonds was applied, as the drugs having fewer rotatable bonds are acceptable [63, 76]. With this filter, 628 molecules were obtained, which were further subjected to molecular docking using the extra precision (XP) mode.

All the molecules were binding to the active site with varying glide scores; hence, a cut-off docking score of -9.0 kcal/mol was chosen for down-selection as it is 2-3 times that of comparables (remdesivir -3.27 kcal/mol; favipiravir -3.44 kcal/mol; molnupiravir -4.93 kcal/mol). Concurrently we also enabled protomerization so that the uncharged BPs can be ionized at pH 7.0 ± 2.0. This is because BPs contain two phosphonate groups attached to a carbon or a nitrogen atom that can undergo ionization depending on the environment's pH. For instance, alendronate, a bone resorption inhibitor used for treating osteoporosis exhibits multi-level ionization for the dissociation of 4-hydroxyl groups present on the phosphorous atom, resulting in a total of 4 dissociation constants at varying pH [77]. Similarly, at a pH ranging from 5 to 9, these BPs may exist as a mixture of protonated or ionized forms. Hence, considering the ionization behaviour at this stage is crucial to evaluate their binding mechanism with the target residues. Therefore, to improve the accuracy and reliability of our docking studies further, and to allow for a comprehensive exploration of ligand's behavior in different biological environments, protomers at pH 7.0 ± 2.0 were generated using Epik module for the top 14 compounds that met the -9.0 kcal/mol docking score cut-off. This resulted in a total of 48 protomers, using which the XP mode of molecular docking was carried out. The list of

247
248

molecules obtained after the cut-off and their corresponding best protomers are shown in Table 1.

249 **Table 1:** Molecular docking results of top 14 bisphosphonate ligands

S. No	ChEMBL ID	Score*	S. No	ChEMBL ID	Score*	S. No	ChEMBL ID	Score*
1	CHEMBL1213265	-10.235 -7.111 [†]	2	CHEMBL608526	-9.706 -8.235 [†]	3	CHEMBL319144	-9.657 -8.010 [†]
4	CHEMBL4802971	-9.355 -8.809 [†]	5	CHEMBL98211	-9.347 -7.956 [†]	6	CHEMBL4291724	-9.308 -6.912 [†]
7	CHEMBL301247	-9.219 -8.150 [†]	8	CHEMBL164344	-9.213 -8.041 [†]	9	CHEMBL300361	-9.151 -8.254 [†]
10	CHEMBL4289996	-9.119 -8.118 [†]	11	CHEMBL387132	-9.11 -8.476 [†]	12	CHEMBL196676	-9.059 -7.558 [†]
13	CHEMBL4569308	-9.02 -8.208 [†]	14	CHEMBL338622	-9.014 -7.938 [†]	15	Cinnamaldehyde (Negative control)	-1.707
16	Remdesivir (Reference drug)	-3.270	17	Favipiravir (Additional reference drug)	-3.443	18	Molnupiravir (Additional reference drug)	-4.927

250 * Represents docking score (in kcal/mol); [†] = protomer form

251

3.1. MM-GBSA studies

252 These top 14 molecules obtained using a cut-off value of <-9.0 kcal/mol from
 253 molecular docking studies, and their respective protomers, were subjected to MM-GBSA
 254 studies to evaluate the binding free energy of the ligand, and the molecules with the least
 255 score when compared to remdesivir were selected. We see that seven candidates which
 256 are either uncharged molecules or charged protomers (highlighted in **bold** font in Table 2
 257 along with their ChEMBL ID's) have lower binding energy than that of remdesivir (-40.32
 258 kcal/mol). For these 7 molecules with lower energy compared to remdesivir, we further
 259 analyzed their interaction pattern as depicted in Figure 2 and Table 3.

260 **Table 2:** MM-GBSA scores of the top-hit bisphosphonate ligands

S. no	Drugs	MM-GBSA dG Bind (kcal/mol)	
		Uncharged state	at pH 7.0 ± 2.0
1.	CHEMBL1213265	-7.74	-33.25
2.	CHEMBL338622	-24.14	-26.52
3.	CHEMBL301247	-24.22	-27.73
4.	CHEMBL4289996	-24.81	-26.97
5.	CHEMBL98211	-26.04	-40.50†
6.	CHEMBL300361	-26.68	-23.47
7.	CHEMBL608526	-33.42	-40.88†
8.	CHEMBL319144	-35.2	-26.39
9.	CHEMBL4802971	-36.77	-39.13
10.	CHEMBL4569308	-40.94†	-43.06†
11.	CHEMBL4291724	-41.51†	-34.06
12.	CHEMBL387132	-43.28†	-38.34
13.	CHEMBL196676	-44.14†	-37.10
14.	CHEMBL164344	-46.65†	-46.73
15.	Favipiravir	-19.13	--
16.	Molnupiravir	-34.13	--
17.	Remdesivir	-40.32	--
18.	Cinnamaldehyde	-30.05	--

261 † MM-GBSA scores lower than that of remdesivir are highlighted in **bold**

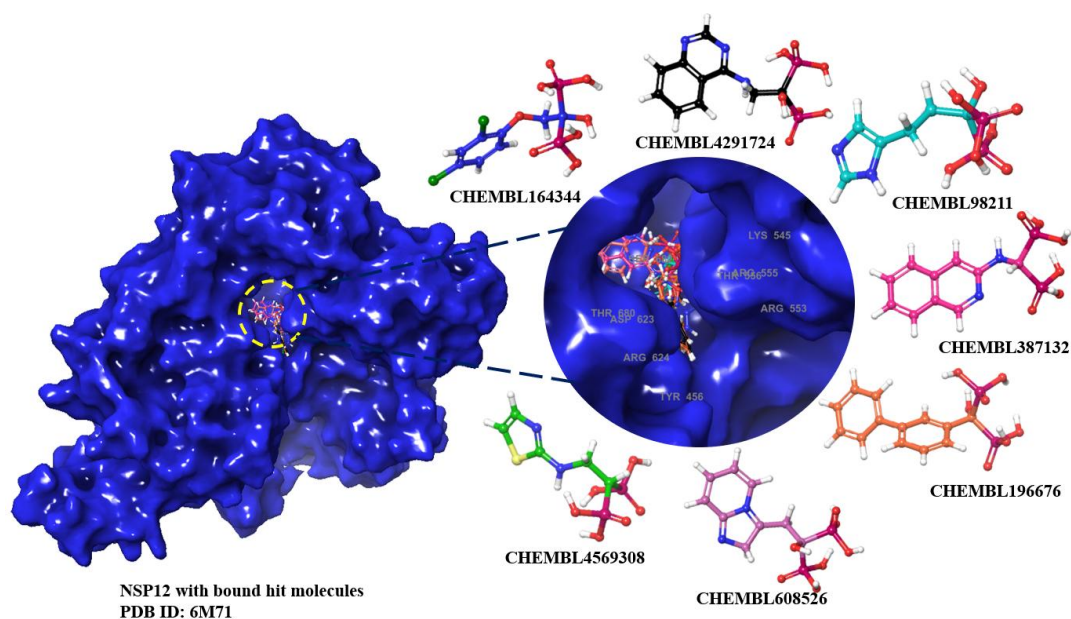


Figure 2: Representation of top hit molecules bound with the target protein (PDB ID: 6M71)

Table 3: Molecular docking results of the hit ligands along with reference drug and a negative control

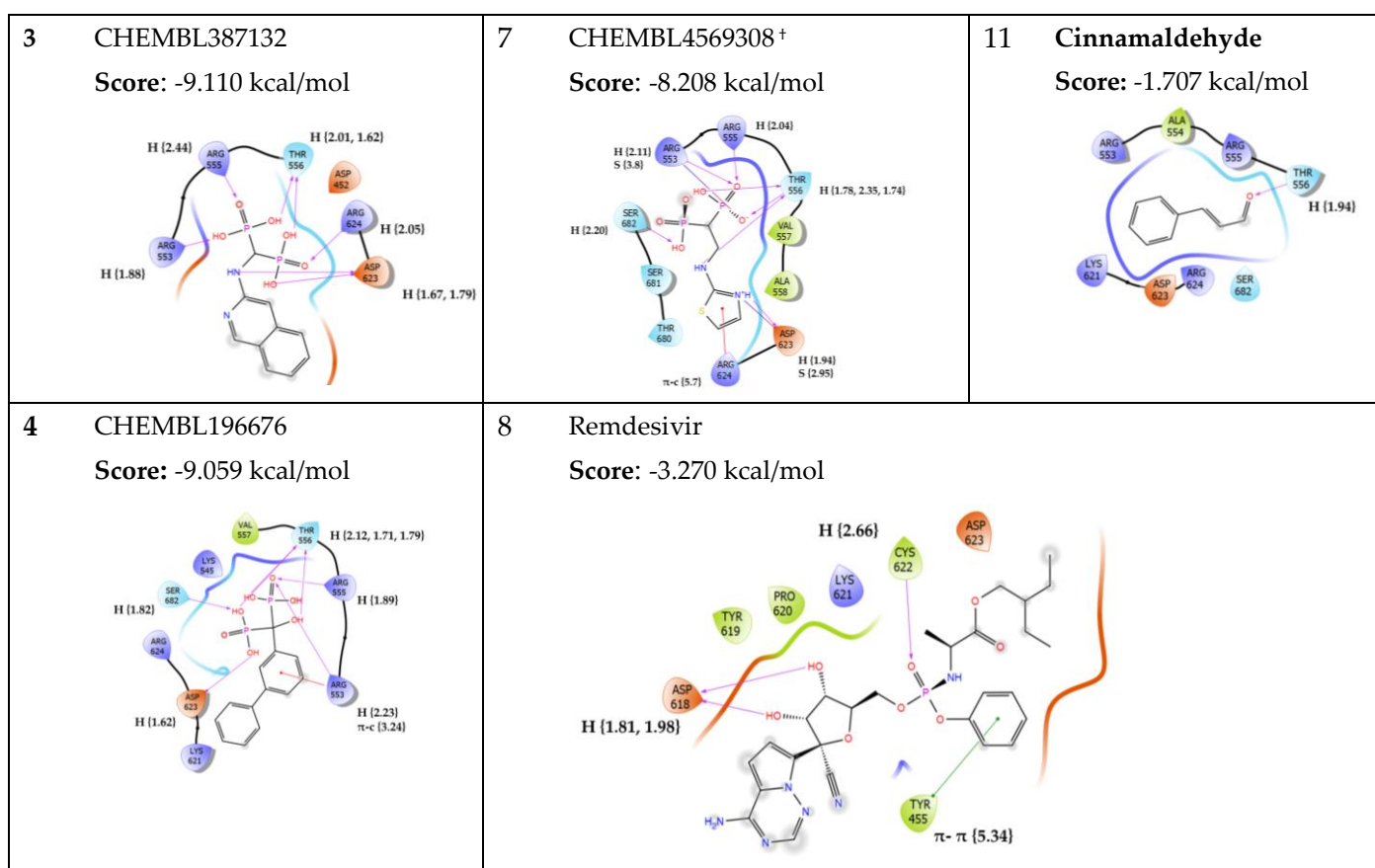
S. No	ChEMBL ID	S. No	ChEMBL ID	S. No	ChEMBL ID
1	CHEMBL4291724 Score: -9.308 kcal/mol	5	CHEMBL608526 ⁺ Score: -8.235 kcal/mol	9	Favipiravir Score: -3.443 kcal/mol
2	CHEMBL164344 Score: -9.213 kcal/mol	6.	CHEMBL98211 ⁺ Score: -7.956 kcal/mol	10	Molnupiravir Score = -4.927 kcal/mol

262

263

264

265



H = Hydrogen bond; S = Salt bridge; π -c = pi-cation; π - π = pi-pi stacking; X = halogen bond; {} = bond length in Å

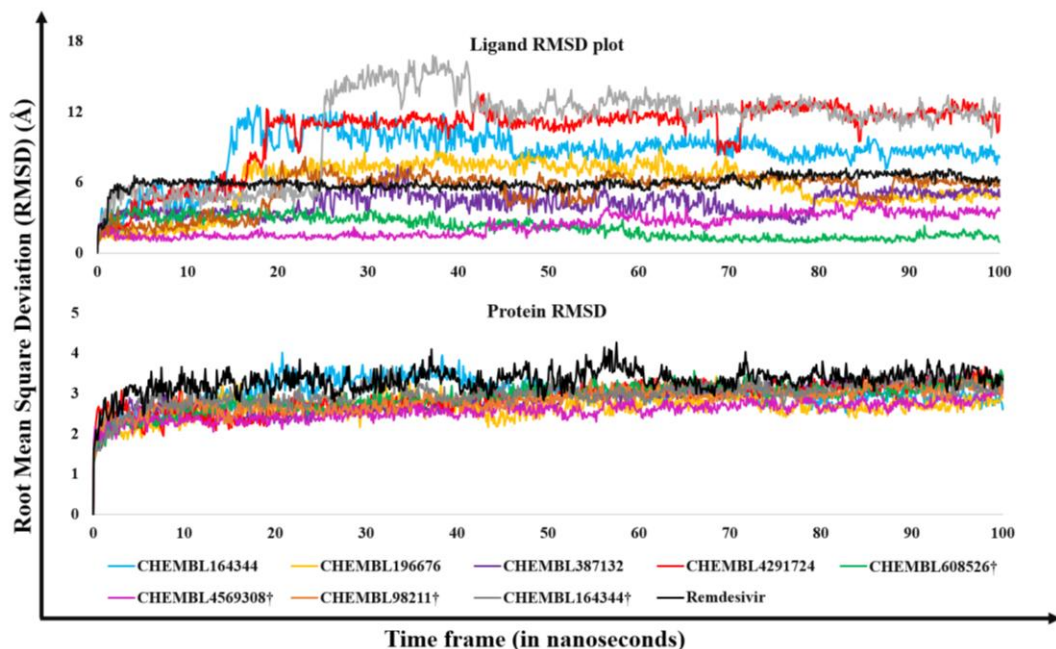
3.2. Molecular dynamics results

The top ligands with the least binding energy from MM-GBSA studies were analyzed by molecular dynamics studies (Figure 3). The clinically used drug remdesivir was also subjected to dynamics simulations for comparative analysis, and showed a stable RMSD plot for the entire duration (5.0 Å–7.0 Å from the initial 5 ns until the end). Additionally, the fluctuations in the active site region of its corresponding protein were low, resulting in a stable RMSD and RMSF plots of the protein (Figures 3 and 4). Significant interactions were observed by the residues of the palm domain that are necessary to bind with the RNA. The residual interactions include Asp618 (63%, water-mediated), Asp623 (70%, water-mediated), and Asp760 (90%, H-bond) (**supplementary file, S1**). In the case of compound CHEMBL164344, the RMSD plot has deviations till 10.0 Å for the initial 18 ns, during which strong interactions were observed with the residues of the palm domain, Thr556, Asp623, and Arg624; later, these interactions gradually decreased, and the interactions with two residues of F domain, Asp452 (81%, H-bond) and Tyr455 (61%, π - π stacking) increased over the time. This has caused a decrease in the RMSD from 12.0 Å at 20th ns to 7.5 Å at 100th ns. In the case of its protomer, the ligand has stable deviations for the initial 25 ns (RMSD 4.0 Å – 6.0 Å), later increasing to 16 Å till 45 ns and then attaining equilibrium until the end with RMSD ranging between 11 Å and 13 Å. The residues that significantly participated in the interactions include Tyr455 (73% π - π stacking, 68% H-bond), Lys551 (69%, H-bond), Arg553 (92%, H-bond), Arg555 (35%, H-bond), and Lys621 (33%, π -cation). It is noted that the protomer's RMSF is similar to that of the uncharged molecule (Figure 4). Change of phoxymethyl (as in CHEMBL164344) with biphenyl group (as in CHEMBL196676) results in significantly more interactions with the residues Asp452 (81%, H-bond) of F domain and Asp623 (85%, H-bond) of palm domain, as well as inconsistent water-mediated interactions with Asp760 (27%). Initially, the in-

266
267
268
269
270
271
272
273
274
275
276
277
278
279
280
281
282
283
284
285
286
287
288
289
290
291

292
293
294
295
296
297

interactions with Arg553, Thr556, and Asp623, as observed in the docked complex, remained for 18 ns, during which no significant deviations were observed (RMSD between 1.0 Å – 3.0 Å); later, the interactions with Asp452, Lys621 along with Asp623 had changed the ligand's conformation, resulting in the increase in the RMSD ranging between 8.0 Å and 7.0 Å which retained till 70 ns, and then a gradual decrease was observed until the end of the simulation (last frame RMSD is 5.4 Å) (Figure 3).



298
299
300

Figure 3: RMSD plot of the hit ligands (above) and the protein (PDB ID: 6M71)

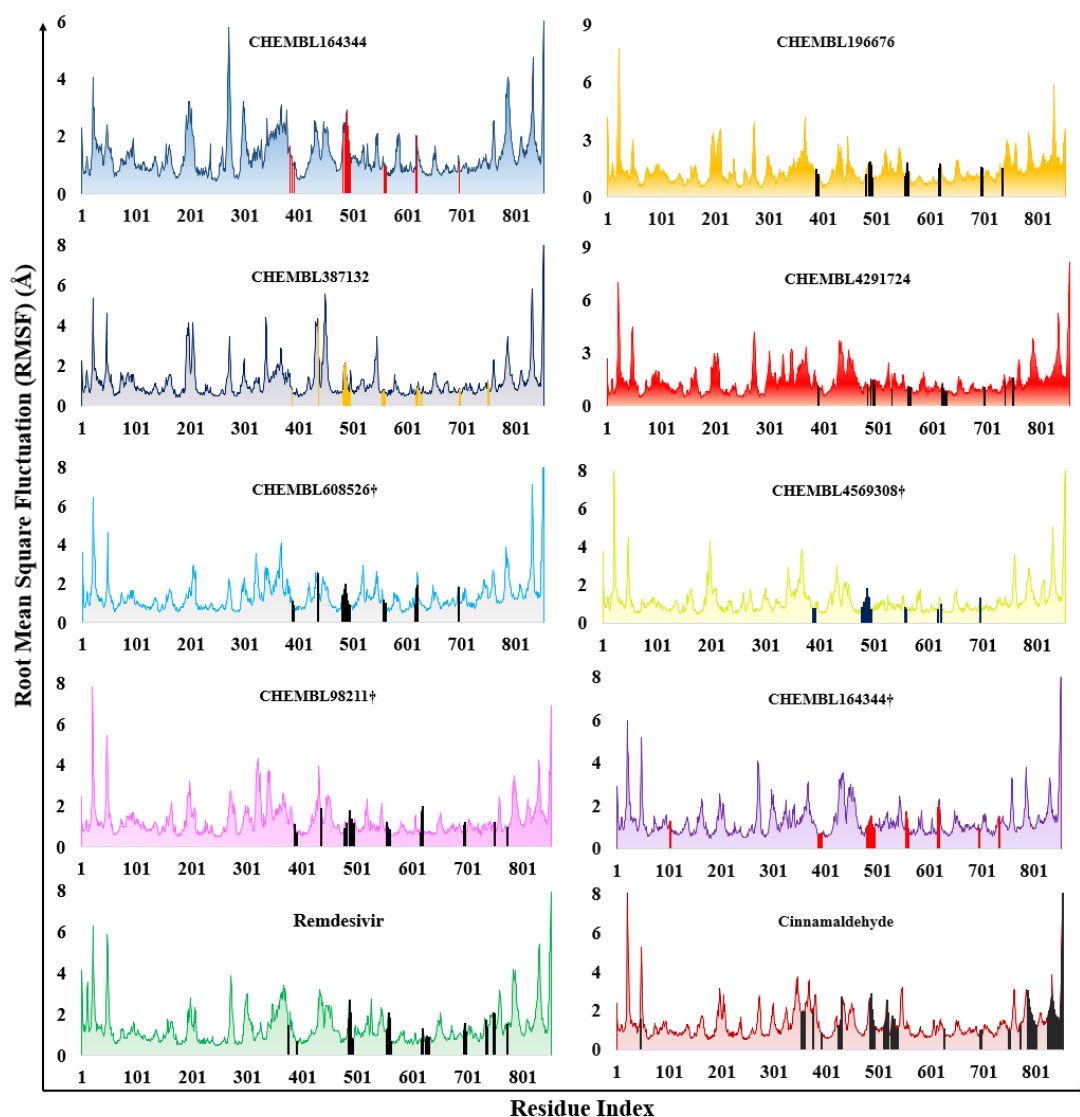


Figure 4: RMSF plot of the protein (PDB ID 6M71) corresponding to top BP ligands, the reference drug (remdesivir) and the negative control (cinnamaldehyde). The fluctuations are shown in colored area plot, while the H-bond interactions are shown as histogram plot within the area. † Indicates protomers.

The quinazoline-4-amine compound (CHEMBL4291724) shows greater stability in terms of its RMSD plot as equilibrium is attained after 20 ns until the end of the simulation with RMSD ranging between 10.0 Å and 12.0 Å (Figure 3). Most of the interactions are between the phosphonic acid groups and the residues of the palm domain, which include Asp623, Thr680, and Asp760, with a contribution of 50%, 39%, and 86%, respectively (**supplementary file, S1**). In the case of CHEMBL387132, a 2-amino isoquinoline compound, the RMSD plot is comparatively lower than other complexes, as the overall deviations for 100 ns were between 3.0 Å and 6.4 Å. Additionally, strong interactions were observed with Asp623 for the first 30 ns and then with Asp760 of the palm domain, contributing to an overall interaction of 30% and 64%, respectively. A residue from the F domain, Lys545, has a total of 33% H-bond interactions with the ligand. (Figure 3, **supplementary file, S1**).

The 2-amino thiazole containing BP (CHEMBL4569308) showed a stable RMSD plot for initial 45 ns (between 1.0 Å and 2.0 Å), had a slight increment over the next few time frames and then attained equilibrium from 60 ns until the end with deviations between 2.5 Å and 4.0 Å. The stability is observed due to the significant involvement of thiazole

301
302
303
304
305
306
307
308
309
310
311
312
313
314
315
316
317
318
319
320

ring in the interactions with Asp623 (99%, H-bond; 71% water-mediated H-bond) and Arg624 (89%, π -cation; 52% and 40% H-bond). Other residues such as Lys545 (68%, H-bond), Arg553 (76%, 82%, H-bond) and Arg555 (68%, 41%, H-bond) showed moderate interactions with the oxygen atoms of the compound. The imidazole compound (CHEMBL98211) attained stability from 20 ns until the end with RMSD between 5.5 Å and 7.0 Å. However, there were slight deviations observed between 45 ns-55 ns and 85 ns-90 ns with RMSD ranging between 4.0 Å and 7.0 Å. These deviations could be due to the intermittent water-mediated interactions with Asp623 (72%). The significantly contributing residues in the interactions include Lys545 (96%, H-bond), Arg555 (77%, 67%, H-bond) and Arg624 (73%, 49%, H-bond) (**supplementary file, S1**). Other residues such as Thr556 and Lys621 contributed with 52% of water-mediated and 48% of H-bond interactions, respectively. The imidazo[1,2- α]pyridine-4-ium compound (CHEMBL608526) exhibited the most stable RMSD plot among all the studied complexes. For the initial 30 ns, its RMSD was between 3.0 Å and 4.0 Å, later there was a gradual decrease until 60 ns, and then equilibrium was attained until the end with RMSD ranging between 1.0 Å and 2.0 Å. There were several residues that significantly contributed to the interactions during the simulation which include Asp450 (91%, H-bond), Lys545 (99%, 68%, H-bond), Arg553 (100%, 99%, H-bond), Arg555 (100%, 93%, H-bond), Asp623 (102%, water-mediated H-bond) and Arg624 (101%, 84%, H-bond interactions). The other residues such as Lys551, Thr556, Ala558 and Ser682 contributed moderately with 63%, 43%, 33% and 60% interactions, respectively. The negative control cinnamaldehyde showed highly unstable RMSD plot with high deviations (up to 90.0 Å), and interactions with <10% contributions (**supplementary file, S1**).

The protein RMSD plot shows a similar pattern of deviations with all the hit ligands, indicating their stability with the ligands during the MD simulation. Similarly, the RMSF plot shows that interacting residues in the active site have acceptable fluctuations (<2.0 Å) (Figure 4). From this, we infer that 5 out of our top 7 ligands behave in a similar fashion to that of remdesivir, with the active site residues forming strong bonds, and most of the interactions by our “hit compounds” attributable to bisphosphonic acid groups. Therefore, there is a good probability that these compounds may emerge as potential RdRp inhibitors if evaluated *in vitro* and/or *ex vivo*.

3.3. Estimation of entropic contribution by gmx_MMPBSA

The MMPBSA analysis helps to understand entropic contribution between protein and ligand during the molecular dynamic simulations [78]. It refers to the degree of randomness in a system and can guide to understand the entropic contributions of the ligand in the active site of the protein. Since MMPBSA analysis module is not available in Schrödinger software, the gmx_MMPBSA tool was used to determine the entropic contributions of the ligands, protein, and the protein-ligand complexes [70]. The change in free energy (ΔG) of the complex is then calculated using the following equation:

$$\Delta G_{binding} = G_{complex} - (G_{protein} + G_{ligand}) \dots\dots\dots (2)$$

$$\Delta G_{binding} = (\Delta E_{MM} - T\Delta S)\dots\dots\dots (3)$$

$$\Delta E_{MM} = (\Delta E_{vdW} + \Delta E_{EL} + \Delta E_{PB} + \Delta E_{NP})\dots\dots\dots (4)$$

In the above equation (1), the $G_{complex}$ represents the free energy of the protein-ligand complex in water, while $G_{protein}$ and G_{ligand} represent the free energies of the protein and ligand respectively in water. The free energy of the total system ($\Delta G_{binding}$) can be obtained by adding the interaction entropy (I.E. = - $T\Delta S$) to the change in total

energy (ΔE_{MM}) of the system [72]. ΔE_{MM} is the summation of various change in energies such as van der Waals (ΔE_{vdW}), electrostatic columbic (ΔE_{EL}), electrostatic potential (ΔE_{PB}) and non-polar (ΔE_{NP}). Applying equation (3), the free energy of the system ($\Delta G_{binding}$) was calculated and tabulated in Table 4 and represented graphically in Figure 5.

Table 4. Entropy results of the top hit compounds showing the entropy contributions, total energies of the system, and the total binding free energies of the ligand at different time frames

Compounds	I.E. = $-T\Delta S$	Total energy contributions (ΔE_{MM})					$\Delta G_{binding}$
		ΔE_{vdW}	ΔE_{EL}	ΔE_{PB}	ΔE_{NP}	$\Delta E_{MM} = \sum \Delta E$	
CHEMBL196676	9.48	-13.06	-90.55	63.70	-2.98	-42.88	-33.41
CHEMBL164344	13.76	-22.77	-93.71	79.14	-3.19	-40.53	-26.77
CHEMBL4291724	15.43	-13.47	-123.47	97.86	-2.73	-41.81	-26.38
CHEMBL387132	20.52	-20.15	-87.58	88.93	-2.88	-21.68	-1.16
CHEMBL608526[†]	29.16	6.03	-620.27	512.53	-3.13	-104.78	-75.62
CHEMBL4569308[†]	34.69	-3.58	-373.84	322.48	-2.71	-57.66	-22.97
CHEMBL164344 [†]	27.45	-11.38	-133.86	107.72	-2.57	-40.10	-12.65
CHEMBL98211 [†]	32.20	1.81	-253.57	222.44	-2.46	-31.78	0.42
Remdesivir	10.86	-52.27	-64.85	92.31	-5.95	-30.77	-19.91
Cinnamaldehyde	6.24	-11.16	-3.24	8.20	-1.03	-7.24	-0.99

I.E. = Interaction entropy; ΔE_{MM} = Total energy contributions of the system; $\Delta G_{binding}$ = binding free energy; [†] protomer form

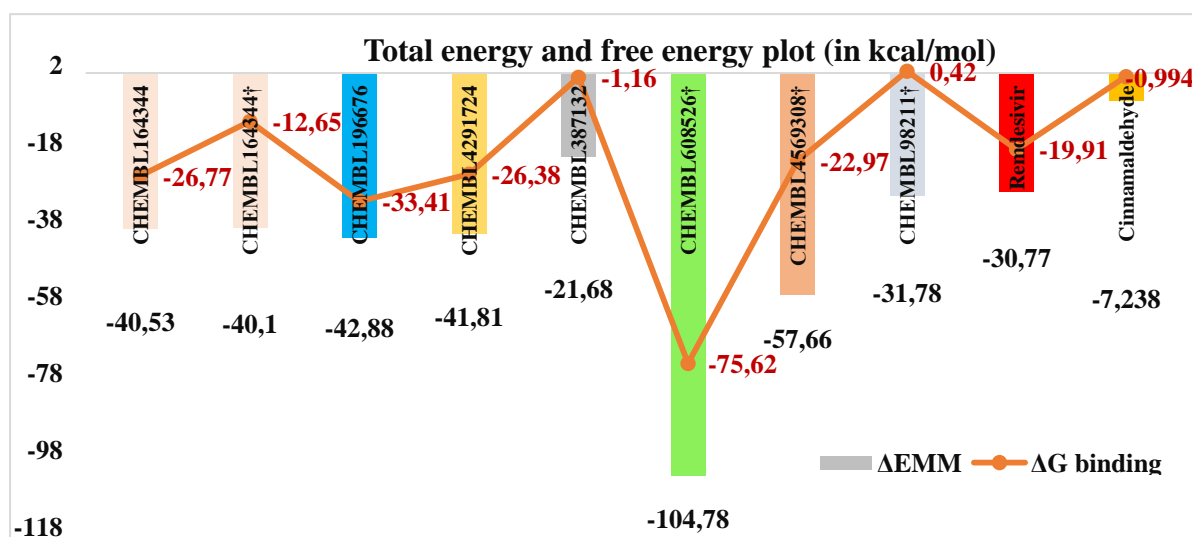


Figure 5. Free energy plot showing the total energies of the system (histogram) and the binding free energies of the hit compounds (line graph) during the dynamics simulations; [†] = protomer form

The results reveal that the protomer of CHEMBL608526 has the least value (-75.62 kcal/mol), while CHEMBL196676 (-33.41 kcal/mol), CHEMBL164344 (-26.77 kcal/mol), CHEMBL4291724 (-26.38 kcal/mol) and CHEMBL4569308 (-22.97 kcal/mol) have values lower than remdesivir (-19.91 kcal/mol). The more negative values signify that the free energy of the complex is lower than the sum of the individual free energies of the protein and the ligand, as seen from equation (2). Therefore, these five candidates, highlighted in **bold** in Table 4, are worth evaluating *in vitro* and/or *ex vivo*. The two other candidates,

386 CHEMBL387132 (-1.16 kcal/mol) and CHEMBL98211 (0.42 kcal/mol), have values close to
387 zero and to the negative control cinnamaldehyde (-0.99 kcal/mol), but they may also be
388 worth evaluating for the following reasons: 1. They perform as well as the 5 highlighted
389 compounds in molecular dynamics studies, showing several interactions with the pro-
390 tein's active site that are absent in the case of negative control (c.f. Figure 3, **supplemen-**
391 **tary file S1**); 2. $\Delta G_{\text{binding}}$ values can vary substantially, e.g. CHEMBL164344's uncharged
392 state value (-26.77 kcal/mol) is twice that of its protomer (-12.65 kcal/mol), therefore it
393 may be premature to dismiss these two compounds; and 3. CHEMBL98211 resembles the
394 approved drug zoledronate which has been observed to benefit COVID-19 human pa-
395 tients as described in section 3.4 below. Although charged molecules are associated with
396 electrostatic repulsions, higher degrees of freedom, and generally lower binding energies
397 leading to more spontaneous binding, we have to exercise caution. This is because the
398 relative contribution of the first term (enthalpy) versus the second term (entropy) in
399 equation (3) is not straightforward in the case of proteins due to conformational effects in
400 the latter and specific properties of a given system [79]. More studies are required with a
401 range of molecules wherein the *in silico* predictions can be experimentally validated to
402 determine whether free energy calculations for charged or uncharged molecules are bet-
403 ter predictive and more useful for drug selection.

404 3.4 Results of *in silico* predicted ADMET profiles

405 All 7 compounds have satisfactory pharmacokinetic and toxicity (ADMET) profiles
406 compared to remdesivir. The intestinal absorption rate ranges from 34% to 72% for all the
407 molecules except for CHEMBL164344 (16.77%). All compounds exhibited similar skin
408 permeability; none acted as a P-glycoprotein (P-gp) substrate. A drug that acts as a sub-
409 strate to P-gp implies low bioavailability, as evident from the studies on remdesivir [80].
410 The volume of distribution in steady state condition ($V_{d_{ss}}$) for all 7 compounds is less
411 except for CHEMBL196676, as the latter possessed better tissue distribution value than
412 remdesivir. The fraction of the drug that remains unbound with blood plasma protein is
413 essential to pass through cell membranes; therefore, higher the fraction unbound (F_u)
414 value, the higher is its distribution [81]. All 7 compounds had better F_u values than
415 remdesivir (0.005 F_u), with CHEMBL608526 showing higher distribution pattern as its
416 value was 0.811 F_u . Due to the presence of phosphonate groups, the compounds are
417 likely to have poor permeability to the blood-brain barrier (BBB) or the central nervous
418 system (CNS); however, CHEMBL387132 and CHEMBL196676 exhibited slightly higher
419 permeability profiles than remdesivir. None of the molecules are likely to be metabolized
420 by cytochrome P450, and all showed a good clearance rate. The maximum tolerated dose
421 is higher than remdesivir and does not inhibit the human ether-a-go-go gene (hERG). The
422 rat oral toxicity levels are higher than remdesivir, indicating high concentrations are re-
423 quired to cause toxicity.

424 The above results, summarized in Table 5, are very promising and indicate that
425 these 7 compounds should be evaluated further, while two of them have a very close
426 similarity to approved drugs. CHEMBL602586 is very similar to minodronic acid, while
427 CHEMBL98211 is close to zoledronic acid (**supplementary file, S1**). Users of BPs, espe-
428 cially alendronate/alendronic acid and zoledronic acid, had "lower odds ratios (OR) of
429 testing for SARS-CoV-2 infection (OR = 0.22; 95%CI:0.21–0.23; $p < 0.001$) COVID-19 diag-
430 nosis (OR = 0.23; 95%CI:0.22–0.24; $p < 0.001$), and COVID-19-related hospitalization (OR =
431 0.26; 95%CI:0.24–0.29; $p < 0.001$)" in a recent study on "whether prior use of BPs is associ-
432 ated with reduced incidence and/or severity of COVID-19" [54,55]. These authors de-
433 cided to investigate BPs (such as alendronate/alendronic acid and zoledronate) because
434 pre-COVID-19 observational studies had reported "decreased in-hospital mortality for
435 patients in the ICU" [82] and "reduced incidence of pneumoniae and pneumonia-related
436 mortality in patients treated with amino-BPs versus controls" [83]. The *in silico* basis for
437 these observations in people using alendronate/alendronic acid is provided by our pre-

vious work [32]; and by this follow up paper for zoledronate and a new drug minodronate. The latter drug and related ChEMBL ID's (Table 4) are worthy of further investigation pertaining to COVID-19 and/or PASC. An *in vitro/ex vivo* analysis similar to McAuley *et al.* [21], or an *in situ* analysis similar to Thompson *et al.* [54], could be faster and useful ahead of *in vivo* studies and clinical trials.

443**Table 5.** Results of *in silico* predicted ADMET profiles of hit bisphosphonate molecules

ADMET parameters				Hit molecules							
ChEMBL →				4291724	164344	387132	196676	98211	608526	4569308	Remdesivir
Absorption	WS (log mol/L)			-2.47	-2.152	-2.046	-3.677	-2.896	-1.444	-1.641	-3.07
	CP (log Papp in 10 ⁻⁶ cm/s)			-0.438	-0.461	0.093	1.245	-0.295	0.334	-0.527	0.635
	IA (% Absorbed)			42.008	16.774	71.627	38.34	24.799	34.854	43.351	71.109
	S.P. (log Kp)			-2.735	-2.743	-2.759	-2.735	-2.735	-2.736	-2.882	-2.735
	P-glyco protein	Substrate		No	No	No	Yes	Yes	No	No	Yes
Inhibitor		I	No	No	No	Yes	No	No	No	Yes	
		II	No	No	No	No	No	No	No	No	No
Distribution	V.D. ss (log L/kg)			-0.768	-0.558	-0.814	0.578	-0.84	-0.439	-0.641	0.307
	F.U. (Fu)			0.331	0.469	0.516	0.028	0.655	0.811	0.6	0.005
	BBB (log BB)			-2.302	-2.284	-1.86	-1.908	-2.489	-1.522	-2.541	-2.056
	CNS (log P.S.)			-4.756	-3.881	-4.034	-3.879	-6.045	-4.881	-4.528	-4.675
Metabolism	CYP action	Substrate	2D6	No	No	No	No	No	No	No	No
			3A4	No	No	No	No	No	No	No	Yes
		Inhibition against 1A2, 2C19, 2C9, 2D6, 3A4		No	No	No	No	No	No	No	No
Excretion	T.C. (log ml/min/kg)			0.146	0.032	-0.025	-0.119	0.664	0.374	0.143	0.198
	ROC			No	No	No	No	No	No	No	No
Toxicity	Ames assay			No	No	No	Yes	No	No	No	No
	MTD (log mg/kg/day)			0.841	0.445	0.689	0.574	-0.312	0.444	1.142	0.15
	hERG I inhibitor			No	No	No	No	No	No	No	No
	hERG II inhibitor			No	No	No	Yes	No	No	No	Yes
	Rat oral toxicity	Acute (LD ₅₀) (mol/kg)		2.67	2.613	1.886	3.117	2.564	2.374	2.738	2.043
		Chronic (LOAEL) (Log mg/kg_bw/day)		3.195	3.597	3.052	3.404	4.773	3.253	3.826	1.639
HT			Yes	No	Yes	No	No	Yes	No	Yes	
SS			No	No	No	No	No	No	No	No	
TT (log ug/L)			0.285	0.285	0.288	0.285	0.285	0.285	0.285	0.285	
MT (log mM)			2.992	1.686	2.938	0.427	2.709	2.355	2.875	0.291	

444 WS: Water Solubility, CP: Caco2 permeability, IA: Intestinal absorption (human), S.P.: Skin Permeability, V.D. ss: Volume of distribution in steady state, F.U.: Fraction unbound (human), T.C.: Total Clearance, ROC: Renal OCT2 substrate, MTD: Max. Tolerated dose
 445 (human), LD₅₀: Lethal dose at 50% concentration, LOAEL: Lowest observed Adverse effect level, HT: Hepatotoxicity, SS: Skin Sensi-
 446 tization, TT: T. Pyriformis toxicity, MT: Minnow toxicity

4. Conclusions

In the current study, *in silico* investigation of BP-containing molecules from the ChEMBL database was carried out. Initial analysis identified 48 molecules with docking scores 2–3 times superior to remdesivir. Subsequent MM-GBSA analysis led to the selection of 7 molecules with notably better free energy scores than remdesivir. These 7 candidates underwent further assessment of their dynamics profiles and entropy calculations, resulting in the identification of 5 promising candidates for *in vitro* evaluation, comprising of 3 uncharged and 2 charged molecules. It is important to consider the charged nature of a molecule to assess protein binding and interactions in biological systems; while its uncharged state could be relevant in the context of stability and metabolism. Notably, our investigation, exemplified by ChEMBL164344, revealed that despite charged and uncharged molecules having similar MM-GBSA scores, dynamic behavior, and total internal energies, their entropy contributions can differ significantly (for example, ChEMBL164344's values were -12.65 kcal/mol for charged and -26.77 kcal/mol for uncharged). Whether it is important to only consider the charged state for down-selection remains to be seen from future experimental and clinical trial observations. The agreement between entropy and dynamics results, combined with *in silico* predicted ADMET analysis, lead us to predict that seven compounds (ChEMBL196676, ChEMBL164344, ChEMBL4291724, ChEMBL608526, ChEMBL4569308, ChEMBL98211, ChEMBL387132) are suitable candidates for synthesis, *in vitro* and *in vivo* evaluation against RdRp. Of these seven, ChEMBL608526 very closely resembles the approved drug minodronate, while ChEMBL98211 resembles the approved drug zoledronate.

Supplementary Materials: Nil

Author Contributions: Conceptualization, M.M.U.-R., M.S., and S.S.V.; methodology, M.M.U.-R., C.K.S., M.G., A.C. and P.V.K.; software, P.V.K., R.P.J., S.R.J.; validation, M.M.U.-R., M.G., M.S., and S.S.V.; formal analysis, M.M.U.-R., C.K.S., M.G., A.C., and P.V.K.; investigation, C.K.S., R.P.J., S.R.J.; resources, M.S., and S.S.V.; data curation, M.M.U.-R., and C.K.S.; writing—original draft preparation, M.M.U.-R., and C.K.S.; writing—review and editing, M.M.U.-R., M.G., M.S., and S.S.V.; visualization, M.M.U.-R., A.C. and M.S.; supervision, M.S., and S.S.V. All authors have read and agreed to the published version of the manuscript

Funding: This research received no external funding.

Institutional Review Board Statement: Not applicable.

Informed Consent Statement: Not applicable.

Data Availability Statement: Any data not provided in this study will be shared upon request.

Acknowledgements: The authors are thankful to the Birla Institute of Technology and Science for providing the necessary facilities to conduct this research, and to the journal and the University of York for defraying the article processing charges.

Conflicts of Interest: The authors declare no conflict of interest.

References

1. Mesel-Lemoine, M.; Millet, J.; Vidalain, P.-O.; Law, H.; Vabret, A.; Lorin, V.; Escriou, N.; Albert, M.L.; Nal, B.; Tangy, F. A Human Coronavirus Responsible for the Common Cold Massively Kills Dendritic Cells but Not Monocytes. *J. Virol.* **2012**, *86*, 7577–7587, doi:10.1128/JVI.00269-12.
2. Zhu, Z.; Lian, X.; Su, X.; Wu, W.; Marraro, G.A.; Zeng, Y. From SARS and MERS to COVID-19: A Brief Summary and Comparison of Severe Acute Respiratory Infections Caused by Three Highly Pathogenic Human Coronaviruses. *Respir. Res.* **2020**, *21*, 224, doi:10.1186/s12931-020-01479-w.
3. WHO Coronavirus (COVID-19) Dashboard. WHO Coronavirus (COVID-19) Dashboard With Vaccination Data. Available online: <https://covid19.who.int/> (accessed on 2 November 2023).

- 496 4. Thaweethai, T.; Jolley, S.E.; Karlson, E.W.; Levitan, E.B.; Levy, B.; Mccomsey, G.A.; Mccorkell, L.; Nadkarni, G.N.;
497 Parthasarathy, S.; Singh, U.; et al. Development of a Definition of Postacute Sequelae of SARS-CoV-2 Infection. *JAMA* **2023**,
498 329, 1934–1946, doi:10.1001/jama.2023.8823.
- 499 5. Proal, A.D.; VanElzakker, M.B. Long COVID or Post-Acute Sequelae of COVID-19 (PASC): An Overview of Biological
500 Factors That May Contribute to Persistent Symptoms. *Front. Microbiol.* **2021**, *12*, 1–24, doi:10.3389/fmicb.2021.698169.
- 501 6. Office for National Statistics (ONS) Prevalence of Ongoing Symptoms Following Coronavirus (COVID-19) Infection in the
502 UK: 2 February 2023 Available online:
503 <https://www.ons.gov.uk/peoplepopulationandcommunity/healthandsocialcare/conditionsanddiseases/bulletins/prevalence>
504 [ofongoingsymptomsfollowingcoronaviruscovid19infectionintheuk/2february2023](https://www.ons.gov.uk/peoplepopulationandcommunity/healthandsocialcare/conditionsanddiseases/bulletins/prevalence) (accessed on 6 November 2023).
- 505 7. Naqvi, A.A.T.; Fatima, K.; Mohammad, T.; Fatima, U.; Singh, I.K.; Singh, A.; Atif, S.M.; Hariprasad, G.; Hasan, G.M.;
506 Hassan, M.I. Insights into SARS-CoV-2 Genome, Structure, Evolution, Pathogenesis and Therapies: Structural Genomics
507 Approach. *Biochim. Biophys. Acta. Mol. basis Dis.* **2020**, *1866*, 165878, doi:10.1016/j.bbadis.2020.165878.
- 508 8. Gao, Y.; Yan, L.; Huang, Y.; Liu, F.; Zhao, Y.; Cao, L.; Wang, T.; Sun, Q.; Ming, Z.; Zhang, L.; et al. Structure of the
509 RNA-Dependent RNA Polymerase from COVID-19 Virus. *Science* **2020**, *368*, 779–782, doi:10.1126/science.abb7498.
- 510 9. Malone, B.; Urakova, N.; Snijder, E.J.; Campbell, E.A. Structures and Functions of Coronavirus Replication–Transcription
511 Complexes and Their Relevance for SARS-CoV-2 Drug Design. *Nat. Rev. Mol. Cell Biol.* **2021**, *23*, 21–39,
512 doi:10.1038/s41580-021-00432-z.
- 513 10. Gangadharan, S.; Ambrose, J.M.; Rajajagadeesan, A.; Kullappan, M.; Patil, S.; Gandhamaneni, S.H.; Veeraraghavan, V.P.;
514 Nakkella, A.K.; Agarwal, A.; Jayaraman, S.; et al. Repurposing of Potential Antiviral Drugs against RNA-Dependent RNA
515 Polymerase of SARS-CoV-2 by Computational Approach. *J. Infect. Public Health* **2022**, *15*, 1180–1191,
516 doi:10.1016/J.JIPH.2022.09.007.
- 517 11. Sivaraman, H.; Er, S.Y.; Choong, Y.K.; Gavor, E.; Sivaraman, J. Structural Basis of SARS-CoV-2- and SARS-CoV-Receptor
518 Binding and Small-Molecule Blockers as Potential Therapeutics. *Annu. Rev. Pharmacol. Toxicol.* **2021**, *61*, 465–493,
519 doi:10.1146/annurev-pharmtox-061220-093932.
- 520 12. Bertolin, A.P.; Weissmann, F.; Zeng, J.; Posse, V.; Milligan, J.C.; Canal, B.; Ulferts, R.; Wu, M.; Drury, L.S.; Howell, M.; et al.
521 Identifying SARS-CoV-2 Antiviral Compounds by Screening for Small Molecule Inhibitors of Nsp12/7/8 RNA-Dependent
522 RNA Polymerase. *Biochem. J.* **2021**, *478*, 2425–2443, doi:10.1042/BCJ20210200.
- 523 13. Baby, K.; Maity, S.; Mehta, C.H.; Suresh, A.; Nayak, U.Y.; Nayak, Y. Targeting SARS-CoV-2 RNA-Dependent RNA
524 Polymerase: An in Silico Drug Repurposing for COVID-19. *F1000Research* **2020**, *9*, 1166, doi:10.12688/f1000research.26359.1.
- 525 14. Kirchdoerfer, R.N.; Ward, A.B. Structure of the SARS-CoV Nsp12 Polymerase Bound to Nsp7 and Nsp8 Co-Factors. *Nat.*
526 *Commun.* **2019**, *10*, 2342, doi:10.1038/s41467-019-10280-3.
- 527 15. Ahmad, J.; Ikram, S.; Ahmad, F.; Rehman, I.U.; Mushtaq, M. SARS-CoV-2 RNA Dependent RNA Polymerase (RdRp) – A
528 Drug Repurposing Study. *Heliyon* **2020**, *6*, e04502, doi:10.1016/j.heliyon.2020.e04502.
- 529 16. El Sohaimy, S.; Abdo, N.; Shehata, M.; Moheyeldin, O. Inhibition of COVID-19 RNA-Dependent RNA Polymerase by
530 Natural Bioactive Compounds: Molecular Docking Analysis. *Egypt. J. Chem.* **2021**, *64*, 1989–2001,
531 doi:10.21608/ejchem.2021.45739.2947.
- 532 17. McDonald, E.G.; Lee, T.C. Nirmatrelvir-Ritonavir for COVID-19. *CMAJ* **2022**, *194*, E218, doi:10.1503/cmaj.220081.
- 533 18. U.S. Food and Drug Administration (FDA) FDA Approves First Oral Antiviral for Treatment of COVID-19 in Adults
534 Available online:
535 <https://www.fda.gov/news-events/press-announcements/fda-approves-first-oral-antiviral-treatment-covid-19-adults>
536 (accessed on 6 November 2023).
- 537 19. Jayk Bernal, A.; Gomes da Silva, M.M.; Musungaie, D.B.; Kovalchuk, E.; Gonzalez, A.; Delos Reyes, V.; Martín-Quirós, A.;

- 538 Caraco, Y.; Williams-Diaz, A.; Brown, M.L.; et al. Molnupiravir for Oral Treatment of Covid-19 in Nonhospitalized Patients.
539 *N. Engl. J. Med.* **2022**, *386*, 509–520, doi:10.1056/NEJMoa2116044.
- 540 20. Manabe, T.; Kambayashi, D.; Akatsu, H.; Kudo, K. Favipiravir for the Treatment of Patients with COVID-19: A Systematic
541 Review and Meta-Analysis. *BMC Infect. Dis.* **2021**, *21*, 489, doi:10.1186/s12879-021-06164-x.
- 542 21. McAuley, A.J.; Vuren, P.J. van; Mohammed, M.-U.-R.; Faheem, F.; Goldie, S.; Riddell, S.; Gödde, N.J.; Styles, I.K.; Bruce,
543 M.P.; Chahal, S.; et al. Use of Human Lung Tissue Models for Screening of Drugs against SARS-CoV-2 Infection. *Viruses*
544 **2022**, *14*, 2417, doi:10.3390/v14112417.
- 545 22. Reis, G.; dos Santos Moreira-Silva, E.A.; Silva, D.C.M.; Thabane, L.; Milagres, A.C.; Ferreira, T.S.; dos Santos, C.V.Q.; de
546 Souza Campos, V.H.; Nogueira, A.M.R.; de Almeida, A.P.F.G.; et al. Effect of Early Treatment with Fluvoxamine on Risk of
547 Emergency Care and Hospitalisation among Patients with COVID-19: The TOGETHER Randomised, Platform Clinical
548 Trial. *Lancet Glob. Heal.* **2022**, *10*, e42–e51, doi:10.1016/S2214-109X(21)00448-4.
- 549 23. Butler, C.C.; Hobbs, F.D.R.; Gbinigie, O.A.; Rahman, N.M.; Hayward, G.; Richards, D.B.; Dorward, J.; Lowe, D.M.; Standing,
550 J.F.; Breuer, J.; et al. Molnupiravir plus Usual Care versus Usual Care Alone as Early Treatment for Adults with COVID-19
551 at Increased Risk of Adverse Outcomes (PANORAMIC): An Open-Label, Platform-Adaptive Randomised Controlled Trial.
552 *Lancet* **2023**, *401*, 281–293, doi:10.1016/S0140-6736(22)02597-1.
- 553 24. Wise, J. Covid-19: Molnupiravir Does Not Cut Hospital Admissions or Deaths in Vaccinated People at High Risk, Trial
554 Finds. *BMJ* **2022**, o3055, doi:10.1136/bmj.o3055.
- 555 25. Kozlov, M. Merck's COVID Pill Loses Its Lustre: What That Means for the Pandemic. *Nature* **2021**,
556 doi:10.1038/d41586-021-03667-0.
- 557 26. Batool, S.; Vuthaluru, K.; Hassan, A.; Bseiso, O.; Tehseen, Z.; Pizzorno, G.; Rodriguez Reyes, Y.; Saleem, F. Efficacy and
558 Safety of Favipiravir in Treating COVID-19 Patients: A Meta-Analysis of Randomized Control Trials. *Cureus* **2023**, *15*,
559 e33676, doi:10.7759/cureus.33676.
- 560 27. Bosaeed, M.; Alharbi, A.; Mahmoud, E.; Alrehily, S.; Bahlaq, M.; Gaifer, Z.; Alturkistani, H.; Alhagan, K.; Alshahrani, S.;
561 Tolbah, A.; et al. Efficacy of Favipiravir in Adults with Mild COVID-19: A Randomized, Double-Blind, Multicentre,
562 Placebo-Controlled Clinical Trial. *Clin. Microbiol. Infect.* **2022**, *28*, 602–608, doi:10.1016/j.cmi.2021.12.026.
- 563 28. Shah, P.L.; Orton, C.M.; Grinsztejn, B.; Donaldson, G.C.; Crabtree Ramirez, B.; Tonkin, J.; Santos, B.R.; Cardoso, S.W.;
564 Ritchie, A.I.; Conway, F.; et al. Favipiravir in Patients Hospitalised with COVID-19 (PIONEER Trial): A Multicentre,
565 Open-Label, Phase 3, Randomised Controlled Trial of Early Intervention versus Standard Care. *Lancet Respir. Med.* **2023**, *11*,
566 415–424, doi:10.1016/S2213-2600(22)00412-X.
- 567 29. Siripongboonsitti, T.; Ungtrakul, T.; Tawinprai, K.; Nimmol, T.; Buttakosa, M.; Sornsamjang, G.; Jarrusrojwuttikul, T.;
568 Silapant, P.; Mahanonda, N. Efficacy of Combination Therapy of Fluvoxamine and Favipiravir vs Favipiravir Monotherapy
569 to Prevent Severe COVID-19 among Mild to Moderate COVID-19 Patients: Open-Label Randomized Controlled Trial
570 (EFFaCo Study). *Int. J. Infect. Dis.* **2023**, *134*, 211–219, doi:10.1016/j.ijid.2023.06.018.
- 571 30. Lenze, E.J.; Mattar, C.; Zorunski, C.F.; Stevens, A.; Schweiger, J.; Nicol, G.E.; Miller, J.P.; Yang, L.; Yingling, M.; Avidan,
572 M.S.; et al. Fluvoxamine vs Placebo and Clinical Deterioration in Outpatients With Symptomatic COVID-19. *JAMA* **2020**,
573 *324*, 2292, doi:10.1001/jama.2020.22760.
- 574 31. Calusic, M.; Marcec, R.; Luksa, L.; Jurkovic, I.; Kovac, N.; Mihaljevic, S.; Likic, R. Safety and Efficacy of Fluvoxamine in
575 COVID-19 ICU Patients: An Open Label, Prospective Cohort Trial with Matched Controls. *Br. J. Clin. Pharmacol.* **2022**, *88*,
576 2065–2073, doi:10.1111/bcp.15126.
- 577 32. Muzaffar-Ur-Rehman, M.; Suryakant, C.K.; Chandu, A.; Kumar, B.K.; Joshi, R.P.; Jadav, S.R.; Sankaranarayanan, M.; Vasan,
578 S.S. Molecular Docking and Dynamics Identify Potential Drugs to Be Repurposed as SARS-CoV-2 Inhibitors. *J. Comput.*
579 *Biophys. Chem.* **2023**, 1–23, doi:10.1142/S2737416523500552. Available at:

580 https://universe.bits-pilani.ac.in/Uploads/Pilani_Upload/Department_of_Pharmacy/Molecular-docking-and-dynamics.pdf
581 (accessed on 26 December 2023).

582 33. Zamzami, M.A. Molecular Docking, Molecular Dynamics Simulation and MM-GBSA Studies of the Activity of
583 Glycyrrhizin Relevant Substructures on SARS-CoV-2 RNA-Dependent-RNA Polymerase. *J. Biomol. Struct. Dyn.* **2023**, *41*,
584 1846–1858, doi:10.1080/07391102.2021.2025147.

585 34. Brunt, D.; Lakernick, P.M.; Wu, C. Discovering New Potential Inhibitors to SARS-CoV-2 RNA Dependent RNA Polymerase
586 (RdRp) Using High Throughput Virtual Screening and Molecular Dynamics Simulations. *Sci. Rep.* **2022**, *12*, 19986,
587 doi:10.1038/s41598-022-24695-4.

588 35. Lu, J.; Lu, W.; Jiang, H.; Yang, C.; Dong, X. Molecular Docking and Dynamics of Phytochemicals From Chinese Herbs With
589 SARS-CoV-2 RdRp. *Nat. Prod. Commun.* **2022**, *17*, 1934578X2211056, doi:10.1177/1934578X221105693.

590 36. Askari, F.S.; Ebrahimi, M.; Parhiz, J.; Hassanpour, M.; Mohebbi, A.; Mirshafiey, A. Digging for the Discovery of
591 SARS-CoV-2 Nsp12 Inhibitors: A Pharmacophore-Based and Molecular Dynamics Simulation Study. *Future Virol.* **2022**, *17*,
592 743–759, doi:10.2217/fvl-2022-0054.

593 37. Uengwetwanit, T.; Chutiwitoonchai, N.; Wichapong, K.; Karoonuthaisiri, N. Identification of Novel SARS-CoV-2 RNA
594 Dependent RNA Polymerase (RdRp) Inhibitors: From in Silico Screening to Experimentally Validated Inhibitory Activity.
595 *Comput. Struct. Biotechnol. J.* **2022**, *20*, 882–890, doi:10.1016/j.csbj.2022.02.001.

596 38. Chinnamadhu, A.; Ramakrishnan, J.; Suresh, S.; Ramadurai, P.; Poomani, K. Dynamics and Binding Affinity of Nucleoside
597 and Non-Nucleoside Inhibitors with RdRp of SARS-CoV-2: A Molecular Screening, Docking, and Molecular Dynamics
598 Simulation Study. *J. Biomol. Struct. Dyn.* **2022**, 1–15, doi:10.1080/07391102.2022.2154844.

599 39. Alzahrani, F.A.; Alkarim, S.A.; Hawsawi, Y.M.; Abdulaal, W.H.; Albiheyri, R.; Kurdi, B.; Alguridi, H.; El-Magd, M.A. 25
600 (S)-Hydroxycholesterol Acts as a Possible Dual Enzymatic Inhibitor of SARS-CoV-2 M pro and RdRp—: An Insight from
601 Molecular Docking and Dynamics Simulation Approaches. *J. Biomol. Struct. Dyn.* **2023**, *41*, 4744–4755,
602 doi:10.1080/07391102.2022.2072392.

603 40. Alexpandi, R.; De Mesquita, J.F.; Pandian, S.K.; Ravi, A.V. Quinolines-Based SARS-CoV-2 3CLpro and RdRp Inhibitors and
604 Spike-RBD-ACE2 Inhibitor for Drug-Repurposing Against COVID-19: An in Silico Analysis. *Front. Microbiol.* **2020**, *11*, 1796,
605 doi:10.3389/fmicb.2020.01796.

606 41. Kushwaha, P.P.; Singh, A.K.; Bansal, T.; Yadav, A.; Prajapati, K.S.; Shuaib, M.; Kumar, S. Identification of Natural Inhibitors
607 Against SARS-CoV-2 Drugable Targets Using Molecular Docking, Molecular Dynamics Simulation, and MM-PBSA
608 Approach. *Front. Cell. Infect. Microbiol.* **2021**, *11*, 730288, doi:10.3389/fcimb.2021.730288.

609 42. Shady, N.H.; Hayallah, A.M.; Mohamed, M.F.A.; Ghoneim, M.M.; Chilingaryan, G.; Al-Sanea, M.M.; Fouad, M.A.; Kamel,
610 M.S.; Abdelmohsen, U.R. Targeting 3CLpro and SARS-CoV-2 RdRp by Amphimedon Sp. Metabolites: A Computational
611 Study. *Molecules* **2021**, *26*, 3775, doi:10.3390/molecules26123775.

612 43. Gajjar, N.D.; Dhameliya, T.M.; Shah, G.B. In Search of RdRp and Mpro Inhibitors against SARS CoV-2: Molecular Docking,
613 Molecular Dynamic Simulations and ADMET Analysis. *J. Mol. Struct.* **2021**, *1239*, 130488,
614 doi:10.1016/j.molstruc.2021.130488.

615 44. Parihar, A.; Sonia, Z.F.; Akter, F.; Ali, M.A.; Hakim, F.T.; Hossain, M.S. Phytochemicals-Based Targeting RdRp and Main
616 Protease of SARS-CoV-2 Using Docking and Steered Molecular Dynamic Simulation: A Promising Therapeutic Approach
617 for Tackling COVID-19. *Comput. Biol. Med.* **2022**, *145*, 105468, doi:10.1016/j.compbio.2022.105468.

618 45. M A Kawsar, S.; Hosen, M.A.; Ahmad, S.; El Bakri, Y.; Laaroussi, H.; Ben Hadda, T.; Almalki, F.A.; Ozeki, Y.; Goumri-Said,
619 S. Potential SARS-CoV-2 RdRp Inhibitors of Cytidine Derivatives: Molecular Docking, Molecular Dynamic Simulations,
620 ADMET, and POM Analyses for the Identification of Pharmacophore Sites. *PLoS One* **2022**, *17*, e0273256,
621 doi:10.1371/journal.pone.0273256.

- 622 46. Veerasamy, R.; Karunakaran, R. Molecular Docking Unveils the Potential of Andrographolide Derivatives against
623 COVID-19: An in Silico Approach. *J. Genet. Eng. Biotechnol.* **2022**, *20*, 58, doi:10.1186/s43141-022-00339-y.
- 624 47. Ribaud, G.; Ongaro, A.; Oselladore, E.; Zagotto, G.; Memo, M.; Gianoncelli, A. A Computational Approach to Drug
625 Repurposing against SARS-CoV-2 RNA Dependent RNA Polymerase (RdRp). *J. Biomol. Struct. Dyn.* **2022**, *40*, 1101–1108,
626 doi:10.1080/07391102.2020.1822209.
- 627 48. Gangadharan, S.; Ambrose, J.M.; Rajajagadeesan, A.; Kullappan, M.; Patil, S.; Gandhamaneni, S.H.; Veeraraghavan, V.P.;
628 Nakkella, A.K.; Agarwal, A.; Jayaraman, S.; et al. Repurposing of Potential Antiviral Drugs against RNA-Dependent RNA
629 Polymerase of SARS-CoV-2 by Computational Approach. *J. Infect. Public Health* **2022**, *15*, 1180–1191,
630 doi:10.1016/j.jiph.2022.09.007.
- 631 49. Hosseini, M.; Chen, W.; Xiao, D.; Wang, C. Computational Molecular Docking and Virtual Screening Revealed Promising
632 SARS-CoV-2 Drugs. *Precis. Clin. Med.* **2021**, *4*, 1–16, doi:10.1093/pccmedi/pbab001.
- 633 50. El Hassab, M.A.; Hemeda, L.R.; Elsayed, Z.M.; Al-Rashood, S.T.; Abdel-Hamid Amin, M.K.; Abdel-Aziz, H.A.; Eldehna,
634 W.M. Computational Prediction of the Potential Target of SARS-CoV-2 Inhibitor Plitidepsin via Molecular Docking,
635 Dynamic Simulations and MM-PBSA Calculations. *Chem. Biodivers.* **2022**, *19*, e202100719, doi:10.1002/cbdv.202100719.
- 636 51. Vesga, L.C.; Ruiz-Hernández, C.A.; Alvarez-Jacome, J.J.; Duque, J.E.; Rincon-Orozco, B.; Mendez-Sanchez, S.C.
637 Repurposing of Four Drugs as Anti-SARS-CoV-2 Agents and Their Interactions with Protein Targets. *Sci. Pharm.* **2022**, *90*,
638 24, doi:10.3390/scipharm90020024.
- 639 52. Elfiky, A.A. Dual Targeting of RdRps of SARS-CoV-2 and the Mucormycosis-Causing Fungus: An in Silico Perspective.
640 *Future Microbiol.* **2022**, *17*, 755–762, doi:10.2217/fmb-2022-0083.
- 641 53. Mohammed, A.O.; Abo-Idrees, M.I.; Makki, A.A.; Ibraheem, W.; Alzain, A.A. Drug Repurposing against Main Protease and
642 RNA-Dependent RNA Polymerase of SARS-CoV-2 Using Molecular Docking, MM-GBSA Calculations and Molecular
643 Dynamics. *Struct. Chem.* **2022**, *33*, 1553–1567, doi:10.1007/s11224-022-01999-9.
- 644 54. Thompson, J.; Wang, Y.; Dreischulte, T.; Barreiro, O.; Gonzalez, R.J.; Hanč, P.; Matysiak, C.; Neely, H.R.; Rottenkolber, M.;
645 Haskell, T.; et al. Association between Bisphosphonate Use and COVID-19 Related Outcomes. *Elife* **2023**, *12*, e79548,
646 doi:10.7554/eLife.79548.
- 647 55. Fumagalli, V.; Iannaccone, M. The Interplay of Drug Therapeutics and Immune Responses to SARS-CoV-2. *Cell. Mol.*
648 *Immunol.* **2023**, doi:10.1038/s41423-023-01098-7.
- 649 56. Wang, B.; Svetlov, D.; Artsimovitch, I. NMPylation and De-NMPylation of SARS-CoV-2 Nsp9 by the NiRAN Domain.
650 *Nucleic Acids Res.* **2021**, *49*, 8822–8835, doi:10.1093/nar/gkab677.
- 651 57. Drake, M.T.; Clarke, B.L.; Khosla, S. Bisphosphonates: Mechanism of Action and Role in Clinical Practice. *Mayo Clin. Proc.*
652 **2008**, *83*, 1032–1045, doi:10.4065/83.9.1032.
- 653 58. Kunzmann, V.; Bauer, E.; Feurle, J.; Tony Florian Weißinger, H.-P.; Wilhelm, M.; Tony, Florian Weißinger, H.-P.; Wilhelm,
654 M. Stimulation of T_H T Cells by Aminobisphosphonates and Induction of Antiplasma Cell Activity in Multiple Myeloma.
655 *Blood* **2000**, *96*, 384–392, doi:10.1182/blood.V96.2.384.
- 656 59. Davies, M.; Nowotka, M.; Papadatos, G.; Dedman, N.; Gaulton, A.; Atkinson, F.; Bellis, L.; Overington, J.P. ChEMBL Web
657 Services: Streamlining Access to Drug Discovery Data and Utilities. *Nucleic Acids Res.* **2015**, *43*, W612–20,
658 doi:10.1093/nar/gkv352.
- 659 60. Friesner, R.A.; Banks, J.L.; Murphy, R.B.; Halgren, T.A.; Klicic, J.J.; Mainz, D.T.; Repasky, M.P.; Knoll, E.H.; Shelley, M.;
660 Perry, J.K.; et al. Glide: A New Approach for Rapid, Accurate Docking and Scoring. 1. Method and Assessment of Docking
661 Accuracy. *J. Med. Chem.* **2004**, *47*, 1739–1749, doi:10.1021/jm0306430.
- 662 61. Shelley, J.C.; Cholleti, A.; Frye, L.L.; Greenwood, J.R.; Timlin, M.R.; Uchimaya, M. Epik: A Software Program for PK(a)
663 Prediction and Protonation State Generation for Drug-like Molecules. *J. Comput. Aided. Mol. Des.* **2007**, *21*, 681–691,

doi:10.1007/s10822-007-9133-z.

62. Koulgi, S.; Jani, V.; Uppuladinne, M.V.N.; Sonavane, U.; Joshi, R. Remdesivir-Bound and Ligand-Free Simulations Reveal the Probable Mechanism of Inhibiting the RNA Dependent RNA Polymerase of Severe Acute Respiratory Syndrome Coronavirus 2. *RSC Adv.* **2020**, *10*, 26792–26803, doi:10.1039/D0RA04743K.

63. Veber, D.F.; Johnson, S.R.; Cheng, H.-Y.; Smith, B.R.; Ward, K.W.; Kopple, K.D. Molecular Properties That Influence the Oral Bioavailability of Drug Candidates. *J. Med. Chem.* **2002**, *45*, 2615–2623, doi:10.1021/jm020017n.

64. Halgren, T.A.; Murphy, R.B.; Friesner, R.A.; Beard, H.S.; Frye, L.L.; Pollard, W.T.; Banks, J.L. Glide: A New Approach for Rapid, Accurate Docking and Scoring. 2. Enrichment Factors in Database Screening. *J. Med. Chem.* **2004**, *47*, 1750–1759, doi:10.1021/jm030644s.

65. Genheden, S.; Ryde, U. The MM/PBSA and MM/GBSA Methods to Estimate Ligand-Binding Affinities. *Expert Opin. Drug Discov.* **2015**, *10*, 449–461, doi:10.1517/17460441.2015.1032936.

66. Karplus, M.; McCammon, J.A. Molecular Dynamics Simulations of Biomolecules. *Nat. Struct. Biol.* **2002**, *9*, 646–652, doi:10.1038/nsb0902-646.

67. Nosé, S. A Unified Formulation of the Constant Temperature Molecular Dynamics Methods. *J. Chem. Phys.* **1984**, *81*, 511–519, doi:10.1063/1.447334.

68. Martyna, G.J.; Tuckerman, M.E.; Tobias, D.J.; Klein, M.L. Explicit Reversible Integrators for Extended Systems Dynamics. *Mol. Phys.* **1996**, *87*, 1117–1157, doi:10.1080/00268979600100761.

69. Mark, P.; Nilsson, L. Structure and Dynamics of the TIP3P, SPC, and SPC/E Water Models at 298 K. *J. Phys. Chem. A* **2001**, *105*, 9954–9960, doi:10.1021/jp003020w.

70. Valdés-Tresanco, M.S.; Valdés-Tresanco, M.E.; Valiente, P.A.; Moreno, E. Gmx_MMPBSA: A New Tool to Perform End-State Free Energy Calculations with GROMACS. *J. Chem. Theory Comput.* **2021**, *17*, 6281–6291, doi:10.1021/acs.jctc.1c00645.

71. Miller, B.R.; McGee, T.D.; Swails, J.M.; Homeyer, N.; Gohlke, H.; Roitberg, A.E. MMPBSA.py : An Efficient Program for End-State Free Energy Calculations. *J. Chem. Theory Comput.* **2012**, *8*, 3314–3321, doi:10.1021/ct300418h.

72. Duan, L.; Liu, X.; Zhang, J.Z.H. Interaction Entropy: A New Paradigm for Highly Efficient and Reliable Computation of Protein-Ligand Binding Free Energy. *J. Am. Chem. Soc.* **2016**, *138*, 5722–5728, doi:10.1021/jacs.6b02682.

73. Shirts, M.R.; Klein, C.; Swails, J.M.; Yin, J.; Gilson, M.K.; Mobley, D.L.; Case, D.A.; Zhong, E.D. Lessons Learned from Comparing Molecular Dynamics Engines on the SAMPL5 Dataset. *J. Comput. Aided. Mol. Des.* **2017**, *31*, 147–161, doi:10.1007/s10822-016-9977-1.

74. Ekberg, V.; Ryde, U. On the Use of Interaction Entropy and Related Methods to Estimate Binding Entropies. *J. Chem. Theory Comput.* **2021**, *17*, 5379–5391, doi:10.1021/acs.jctc.1c00374.

75. Pires, D.E. V.; Blundell, T.L.; Ascher, D.B. PkCSM: Predicting Small-Molecule Pharmacokinetic and Toxicity Properties Using Graph-Based Signatures. *J. Med. Chem.* **2015**, *58*, 4066–4072, doi:10.1021/acs.jmedchem.5b00104.

76. Dutta, K.; Shityakov, S.; Morozova, O.; Khalifa, I.; Zhang, J.; Zhu, W.; Panda, A.; Ghosh, C. Beclabuvir Can Inhibit the RNA-Dependent RNA Polymerase of Newly Emerged Novel Coronavirus (SARS-CoV-2). *Preprint* **2020**, doi:10.20944/preprints202003.0395.v2.

77. Ke, J.; Dou, H.; Zhang, X.; Uhagaze, D.S.; Ding, X.; Dong, Y. Determination of PKa Values of Alendronate Sodium in Aqueous Solution by Piecewise Linear Regression Based on Acid-Base Potentiometric Titration. *J. Pharm. Anal.* **2016**, *6*, 404–409, doi:10.1016/j.jpha.2016.07.001.

78. Homeyer, N.; Gohlke, H. Free Energy Calculations by the Molecular Mechanics Poisson–Boltzmann Surface Area Method. *Mol. Inform.* **2012**, *31*, 114–122, doi:10.1002/minf.201100135.

79. MacRaild, C.A.; Daranas, A.H.; Bronowska, A.; Homans, S.W. Global Changes in Local Protein Dynamics Reduce the

706 Entropic Cost of Carbohydrate Binding in the Arabinose-Binding Protein. *J. Mol. Biol.* **2007**, *368*, 822–832,
707 doi:10.1016/j.jmb.2007.02.055.

708 80. Jorgensen, S.C.J.; Kebriaei, R.; Dresser, L.D. Remdesivir: Review of Pharmacology, Pre-clinical Data, and Emerging Clinical
709 Experience for COVID-19. *Pharmacother. J. Hum. Pharmacol. Drug Ther.* **2020**, *40*, 659–671, doi:10.1002/phar.2429.

710 81. Cervelli, M.J.; Russ, G.R. Principles of Drug Therapy, Dosing, and Prescribing in Chronic Kidney Disease and Renal
711 Replacement Therapy. In *Comprehensive Clinical Nephrology*; Elsevier, 2010; pp. 871–893 ISBN 9780323077668.

712 82. Lee, P.; Ng, C.; Slattery, A.; Nair, P.; Eisman, J.A.; Center, J.R. Preadmission Bisphosphonate and Mortality in Critically Ill
713 Patients. *J. Clin. Endocrinol. Metab.* **2016**, *101*, 1945–1953, doi:10.1210/jc.2015-3467.

714 83. Sing, C.; Kiel, D.P.; Hubbard, R.B.; Lau, W.C.; Li, G.H.; Kung, A.W.; Wong, I.C.; Cheung, C. Nitrogen-Containing
715 Bisphosphonates Are Associated With Reduced Risk of Pneumonia in Patients With Hip Fracture. *J. Bone Miner. Res.* **2020**,
716 *35*, 1676–1684, doi:10.1002/jbmr.4030.

717
718 **Disclaimer/Publisher’s Note:** The statements, opinions and data contained in all publications are solely those of the individual
719 author(s) and contributor(s) and not of MDPI and/or the editor(s). MDPI and/or the editor(s) disclaim responsibility for any
720 injury to people or property resulting from any ideas, methods, instructions or products referred to in the content.